Experimental investigation of kinematic pile bending in layered soils using dynamic centrifuge modelling

Thejesh Kumar Garala[*], Gopal S.P. Madabhushi[†] and Raffaele Di Laora[‡]

ABSTRACT

This research provides an insight into the previously unexplored aspects of kinematic pile bending, especially for large intensity earthquakes where the soil behaviour is highly non-linear. In this study, a series of dynamic centrifuge experiments were conducted on pile foundations embedded in a two-layered soil profile to investigate the kinematic loads acting on the pile foundations during model earthquakes. Single pile and a closely spaced 3×1 row pile group were used as model pile foundations, and the soil model consisted of a soft clay underlain by dense sand. It was observed that the peak kinematic pile bending moment occurs slightly beneath the interface of soil layers and this depth is larger for the pile group compared to a single pile. Also, the piles in a group attract lower bending moments but carry larger residual kinematic pile bending moments compared to a single pile. Further, the elastic solutions available in the literature for estimating the kinematic pile bending moments are shown to yield satisfactory results only for small intensity earthquakes, but vastly under-estimate for large intensity earthquakes. The importance of considering soil non-linearity effects and accurate determination of shear strain at the interface of layered soils during large intensity earthquakes for a reliable assessment of kinematic pile bending moment from literature methods is demonstrated using dynamic centrifuge test data.

KEYWORDS: centrifuge; earthquakes; kinematic interaction; layered soil; pile bending moment; pile group; single pile

[*] PhD Student, Schofield Centre, Department of Engineering, University of Cambridge, UK.
Email: tkg24@cam.ac.uk

[†] Professor of Civil Engineering & Director of Schofield Centre, Department of Engineering, University of Cambridge, UK.
Email: mspg1@cam.ac.uk

[‡] Assistant Professor, Department of Engineering, Università della Campania Luigi Vanvitelli, Aversa, Italy.
Email: raffaele.dilaora@unicampania.it

PROBLEM DESCRIPTION

Pile foundations are widely used on land and offshore to transfer heavy superstructure loads to deeper, competent layers of soil, relying on both skin-friction and tip resistance. During the earthquakes, the lateral shaking of surrounding soil induces additional forces (kinematic interaction) on pile foundations along with the forces imposed by the vibrations of the superstructure (inertial interaction). These phenomena occur simultaneously and are therefore difficult to separate. Several post-earthquake field investigations indicate that most of the pile foundations fail at shallow depths of the pile, indicating the inability of the piles to transfer large inertial forces that arose during earthquakes. Nevertheless, there are few cases where the pile foundation failure was observed at deeper locations indicating the dominance of kinematic effects, as inertial bending is insignificant at such depths (Mizuno, 1985; Gazetas et al., 1993). Pile failure under kinematic loads can occur due to the lateral spreading of liquefied soil, but also due to the kinematic interaction: (a) close to the pile head in a very soft soil and (b) at the interface between the two soil layers of strongly differing stiffness. While the effects of lateral spreading have received significant attention (Haigh, 2002; Brandenberg et al., 2005; Madabhushi et al., 2010; Haskell, 2013), there is a paucity of experimental research on kinematic interaction.

Many of the seismic design codes still recommend the design of pile foundations based only on inertial loads. However, EC8 (EN 1998-5:2004) highlights the importance of kinematic loads and recommends the consideration of kinematic loads in the design of piles and piers under certain conditions. Although there are some discussions regarding the correlation between these conditions and the relevance of kinematic effects (see for example, de Sanctis & Di Laora, 2017), this lies beyond the scope of the paper. As a matter of fact, there are no specific recommendations in EC8 on the procedure to be adopted for computing the kinematic loads acting on the pile foundations. Since the mid-1960s, several researchers tried to understand the inertial and kinematic loads effect on pile foundations using sub-structure method, Winkler analyses with linear-elastic or hysteretic soil behaviour, finite element or boundary element analyses and model scale laboratory tests. Novak (1991) and Gazetas & Mylonakis (1998) reviewed the then state-of-the-art research. Later, Nikolaou et al. (2001), Mylonakis (2001), Maiorano et al. (2009), Di Laora et al. (2012) and recently, Mucciacciaro & Sica (2018), among others,

studied the kinematic pile bending response at the interface of two-layer soils and proposed equations for determining the kinematic pile bending moments (M_k). These will be discussed in detail later in this paper.

The above solutions consider the soil behaviour as linear elastic or linear visco-elastic and are applicable only for a single pile. This raises a concern regarding application of the above methods in practice, as the EC8 recommends considering kinematic effects only in the zones of moderate or high seismicity, i.e. with $a_g S > 0.10$g, where a_g is the design ground acceleration (function of importance factor and reference peak ground acceleration on type 'A' ground) and S is a soil factor. Under such conditions, the soil behaviour is expected to be non-linear with some plastic strain mobilisation and not linear elastic. Therefore, the existing methods in literature to determine the M_k need to be evaluated against experimental data to check their validity for a wide range of earthquake intensities and eventually adapt the methods accounting for soil and pile nonlinearity. Further, a large amount of numerical evidence (e.g. Fan et al., 1991) and limited field evidence (Nikolaou et al., 2001) suggests that group effects for kinematic loading in pile foundations are not significant. However, there is a need to corroborate the assumption of minimal pile group effects during kinematic pile bending and to understand additional group effects on M_k in piles of a pile group using well-controlled laboratory experiments.

In this research, a series of dynamic centrifuge experiments were carried out on pile foundations embedded in two-layer soil strata to investigate the effects of kinematic loading on pile foundations during earthquakes of different intensities. The soil profile consists of a soft kaolin clay layer overlying a dense, fraction-B Leighton Buzzard (LB) sand. A model single pile (SP) and a 3×1 row pile group (PG) were tested in this study. Pile caps made from acrylic Perspex were used to replicate the cap effects but with no significant inertial effects on the pile foundations due to the negligible mass of the Perspex. This paper initially discusses the engineering properties of the soil and pile foundations followed by their dynamic behaviour. Later, the experimental observations on M_k in the single pile and pile group are presented. Finally, experimentally determined M_k results are compared with the literature methods, with and without the soil non-linearity effects.

EXPERIMENTAL SETUP

Physical modelling using the centrifuge

Field stress-strain conditions can be replicated in a scaled-down model of a geotechnical structure by subjecting the model to increased g-field using a centrifuge. The principles of centrifuge modelling are well discussed in Schofield (1980) and Madabhushi (2014). In this research, the Turner beam centrifuge at Schofield Centre, University of Cambridge, was used to test the scaled centrifuge models at 60*g*. Equivalent shear beam (ESB) box (Brennan & Madabhushi, 2002) was used as a container to prepare the model and the servo-hydraulic shaker developed by Madabhushi et al. (2012) was used to fire the required model earthquakes.

Materials

The soil model was prepared with dense, poorly graded, fraction-B Leighton Buzzard (LB) sand underlying the soft speswhite kaolin clay to maintain significant stiffness contrast between the soil layers. Table 1 gives the properties of fraction-B LB sand that were experimentally determined following appropriate standards. Laboratory grade speswhite kaolin clay is widely used in many experimental campaigns in Cambridge. The properties of speswhite kaolin clay (Lau, 2015) are given in Table 2.

Model pile foundations

An aluminium (Alloy 6061 T6) tubular model pile of outer diameter (d) 11.1 mm and thickness (t) 0.9 mm was used in this study to fabricate a single pile (SP) and a 3×1 row pile group (PG) configuration. A pile spacing of 3d centre-to-centre was used for the piles in the pile group, as it is the minimum pile spacing recommended by BS 8004 (2015) for the circular friction piles in a group. The bottom of tubular piles is closed with an aluminium plug to restrict the entry of soil into the piles during pile installation. Table 3 shows the equivalent prototype characteristics of a single pile.

The single pile and the end piles of the pile group were strain gauged to measure the bending moments during earthquakes. Caps made from acrylic Perspex were used as pile caps for both single pile and pile group. Mass of single pile and pile group Perspex caps are 11 and 24 grams respectively

and these are negligible in comparison to the self-weight of the pile. Hence, the measurements (accelerations and bending moments) during the earthquakes can be considered as the effect of soil (kinematic effect) alone on the pile foundations. Figure 1 shows the schematic view of pile foundations used in the study along with the location of strain gauges.

Table 1. Properties of fraction-B Leighton Buzzard (LB) sand

Property	Standard	Value
Specific gravity, G_s	ASTM D854 (2014)	2.65
Maximum void ratio, e_{max}	ASTM D4254 (2016)	0.767
Minimum void ratio, e_{min}	ASTM D4253 (2016)	0.49
Effective particle size, D_{10} (mm)	ASTM D6913 (2017)	0.68
Average particle size, D_{50} (mm)	ASTM D6913 (2017)	0.80
Coefficient of uniformity, C_u	ASTM D6913 (2017)	1.221
Coefficient of curvature, C_c	ASTM D6913 (2017)	0.97
Relative density, D_r (%)	ASTM D4254 (2016)	85
Peak friction angle, ϕ_p (°)	ASTM D7181 (2011)	37.2

Table 2. Properties of speswhite kaolin clay (Lau, 2015)

Property	Value
Plastic limit, *PL* (%)	30
Liquid limit, *LL* (%)	63
Plasticity index, *PI* (%)	33
Specific gravity, G_s	2.60
Slope of critical state line (CSL) in q-p' plane	0.90
Slope of an unload-reload line, (κ)	0.039
Intercept of CSL at p'=1 kPa (Γ)	3.31
Slope of normal consolidation line (λ)	0.22

Table 3. Equivalent prototype characteristics of a model single pile

Property	Model scale	Prototype scale	Equivalent field case
Material	Aluminium alloy	Aluminium alloy	Reinforced concrete pile
Outer diameter	11.1 mm	0.666 m	0.695 m
Thickness	0.9 mm	0.054 m	Solid section
Length	300 mm	18 m	18 m
Young's modulus	70 GPa	70 GPa	30 GPa
Flexural rigidity	2.65×10^{-05} MN-m^2	344 MN-m^2	344 MN-m^2
Yield strength	305 MPa	305 MPa	28 MPa
Elastic yield moment capacity	20.43×10^{-03} kN-m	4414 kN-m	923 kN-m

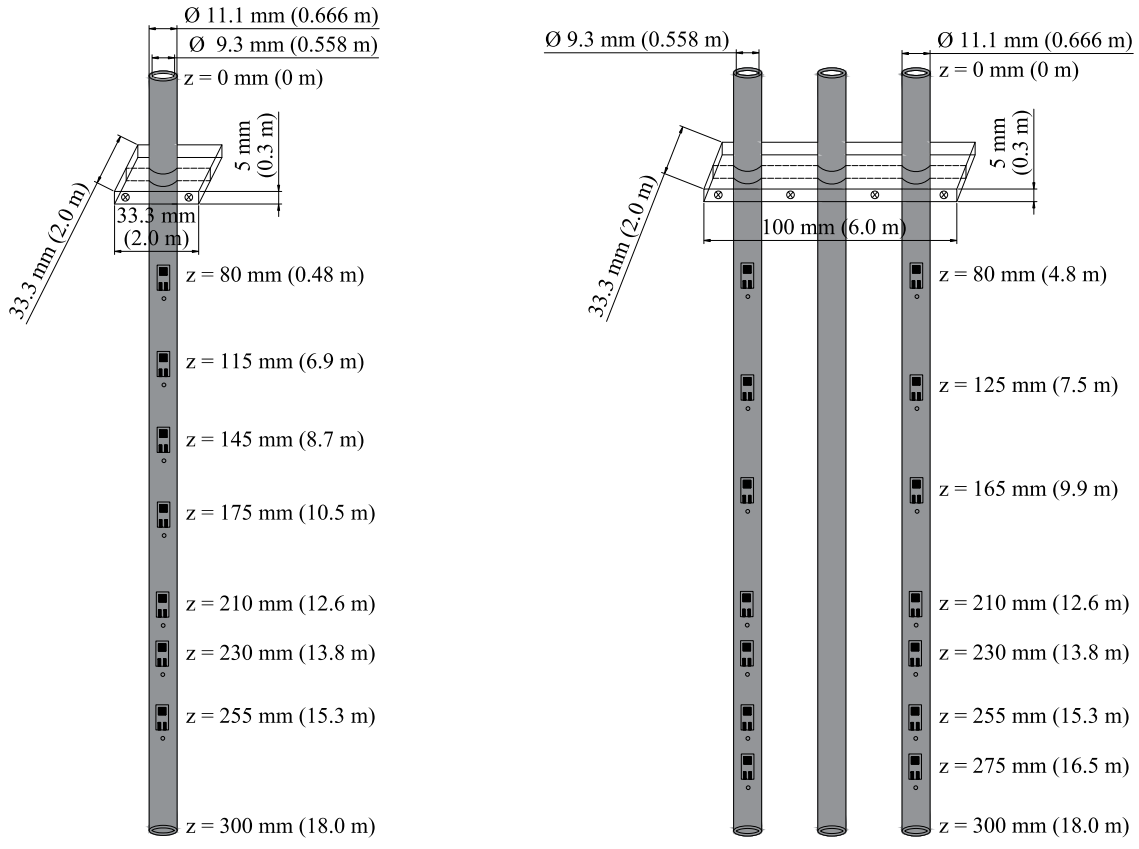

Fig. 1. Pile foundations considered in the study (a) Single pile - SP (b) Pile group - PG

Model preparation

The sand layer was prepared at 1*g* by pouring the sand into the ESB box following the air-pluviation method using an automatic sand pouring machine (Madabhushi et al., 2006). The sand layer was saturated using the de-aired water with 5~10 mm of extra water at the top of the sand bed to minimise any air entry during the clay pouring. Clay slurry was prepared by mixing the speswhite kaolin clay powder and de-aired water in the ratio of 1:1.25 under vacuum. The ESB box with clay slurry and the sand layer was placed under a computer-controlled hydraulic press to consolidate the clay slurry under a vertical stress of around 125 kPa. The vertical stress was applied to achieve an average undrained shear strength of about 10~15 kPa in the clay layer. During the unloading phase of the consolidation, the clay was always maintained under a suction of -60 kPa to -70 kPa by not allowing sufficient amount of water back into the model. These suction pressures in clay are well below the air entry value of kaolin clay and hence, no cavitation can occur. The suction pressures will create higher effective vertical stresses in the clay layer, however, the suction in clay can continue to drop at a slower rate until spinning of the model in centrifuge due to possible absorption of water from the saturated sand layer.

The depth of clay layer after consolidation and trimming was 150 mm with a saturated unit weight of 16.2 kN/m^3. Pile foundations were installed manually at 1*g* with piles being gently pushed into the clay at an approximate rate of 2~4 mm/sec. A manual hydraulic jack was used to embed the piles into the sand up to a depth of 80 mm (~7.20*d*) at an approximate rate of 0.5~1 mm/sec. Piezoelectric accelerometers (PAs) and micro-electro-mechanical systems accelerometers (MEMSs) were used to measure the accelerations in the soil model and pile foundations respectively. Figure 2 shows the plan view of the model and Fig. 3 shows the cross-section of the model along with the instrument locations. The dimensions in Figs. 1 to 3 are at model scale, and the values within the parentheses represent the prototype dimensions. The pile caps (see Fig. 1) are located at 20 mm above the clay surface as shown in Fig. 3. Single pile and pile group were sited on different vertical planes in the direction of shaking and hence the dynamic interaction between the two will be very minimal. Moreover, the piezoelectric accelerometers were placed on a different vertical plane and reasonably far from the pile foundations

(see Fig. 2). Therefore, the response from piezoelectric accelerometers can be considered as far-field soil response (Garala & Madabhushi, 2019).

The thickness of soil layers was governed by the ESB box dimensions. The top and bottom soil layers possess a thickness of 13.5d and 11.7d respectively, which should be sufficient to mobilise significant kinematic effects on the pile foundations. Further, the bottom soil layer thickness must be sufficient to provide adequate fixity to the pile and any depth beyond that is not going to influence the M_k at the interface. Piles were embedded up to a depth of 7.2d in the sand layer, and according to Dezi et al. (2008) and Haskell (2013), this should generate significant interface effects on the pile foundations. Also, the distance from pile toes to the bottom of the sand bed is around 4.5d, but according to Nikolaou et al. (1995) this distance has insignificant effect on the M_k at the interface.

Centrifuge testing

The model was swung up to 60g in increments of 10g with bottom drain closed in the centrifuge. During the swing up process of the centrifuge, the suction pressures developed in the clay layer after unloading from the hydraulic press reduce, due to an increase in the body forces which create larger total stresses. These larger total stresses will partly create excess pore pressures and partially satisfy the suction pressures present in clay. Further, the effective stresses are high before the start of the centrifuge due to the suction pressures in the clay. However, these remain constant during the swing up process and only increase with the onset of excess pore pressure dissipation during the consolidation phase. No additional water could flow into the model in the centrifuge. This procedure was adopted to obtain a relatively soft clay profile in the test. On the other hand, the effective stresses in the sand layer will be small at 1g and increase with the g level in the centrifuge. Once the model attains equilibrium at 60g, a T-bar test and shear wave velocity (v_s) profiling were conducted, and then the planned model earthquakes (hereafter called as base excitations (BEs)) were fired using the servo-hydraulic shaker in the same sequence as shown in Fig. 4. BE1 to BE4 excitations have 10 cycles of sinusoidal loading with various frequencies and BE5 is a scaled 1995 Kobe earthquake motion. The excitations considered enable to understand the kinematic loads on the pile foundations for a variety of shaking intensities.

The following sections present the important research outcomes, in which the results are discussed at prototype scale, unless stated otherwise.

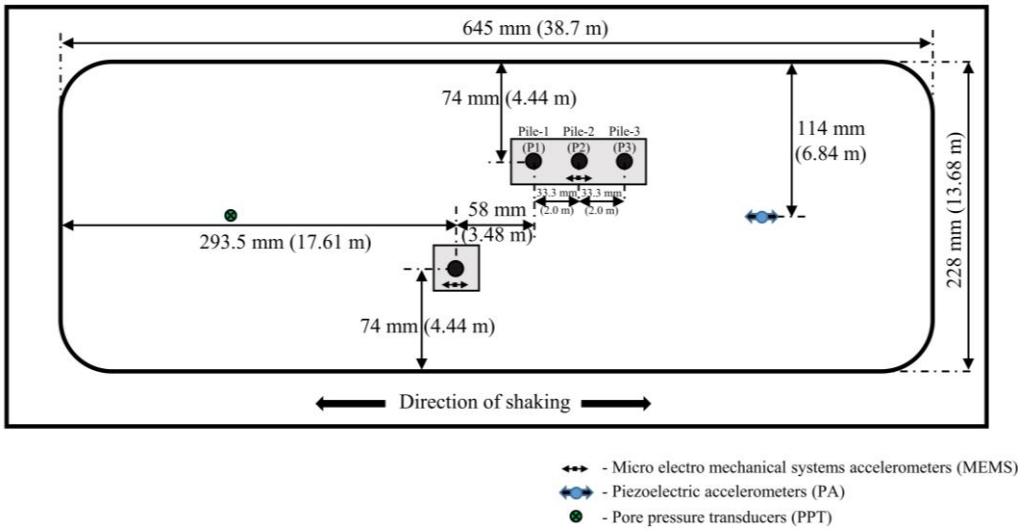

Fig. 2. Plan view of the centrifuge model

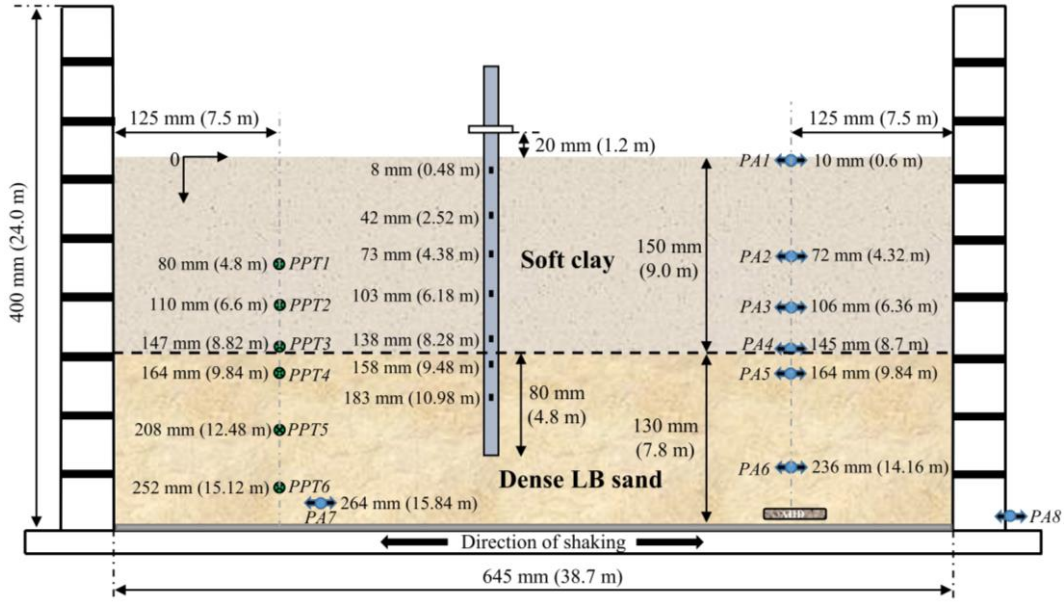

Fig. 3. Cross-sectional view of the centrifuge model

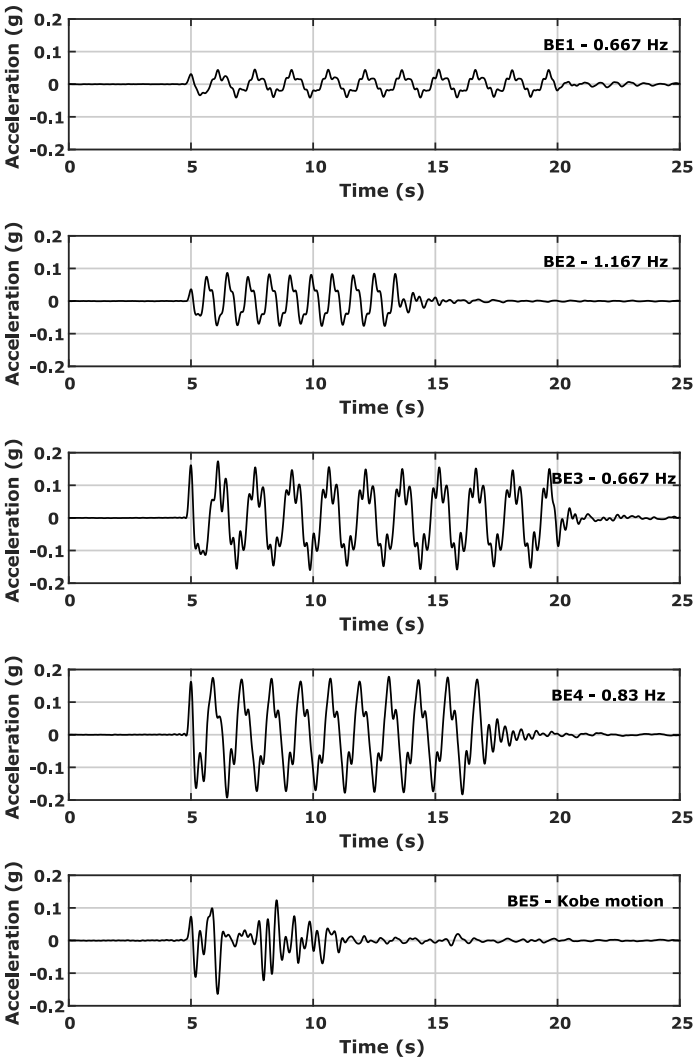

Fig. 4. Base excitations considered in the study (at prototype scale)

STRENGTH AND STIFFNESS OF THE SOIL LAYERS

T-bar test (Lau, 2015) was performed on the clay layer at 60*g* before firing the base excitations to determine the undrained shear strength (c_u) of the clay. The T-bar used in this study was 40 mm wide, 4 mm in diameter and the rate of penetration was approximately 1.7~1.9 mm/sec. The penetration resistance (q) measured by the T-bar is converted into c_u using 10.5 as the T-bar bearing factor, N_T ($=q/c_u$), following the recommendation of Randolph & Houlsby (1984). Figure 5a shows the c_u profile of the clay tested. Further, the shear wave velocity (v_s) at different depths was evaluated from the air hammer device (Ghosh & Madabhushi, 2002). Maximum shear modulus (G_0) was determined from the measured v_s using the equation (1), where ρ is the mass density of the corresponding soil layer.

$$G_0 = \rho v_s^2 \qquad (1)$$

G_0 obtained at different depths before firing the base excitations are shown in Fig. 5b. Also, G_0 of soil layers tested were computed from Hardin & Drnevich (1972) (equation 2), Viggiani & Atkinson (1995) (equation 3) and Oztoprak & Bolton (2013) (equation 4) at the known pore water pressure locations (see Fig. 3) and shown in Fig. 5b.

$$\frac{G_0}{p_r} = 3300\frac{(2.973-e)^2}{1+e}OCR^{0.25}\left(\frac{p'}{p_r}\right)^{0.50} \quad (2)$$

$$\frac{G_0}{p_r} = 950\left(\frac{p'}{p_r}\right)^{0.8}OCR^{0.24} \quad (3)$$

$$\frac{G_0}{p_{ref}} = \frac{5520}{(1+e)^3}\left(\frac{p'}{p_{ref}}\right)^{0.51} \quad (4)$$

In equations 2-4, p' is the mean effective stress, e is the void ratio, OCR is the over-consolidation ratio, p_r and p_{ref} are reference pressures of 1 kPa and 100 kPa respectively. The fitting parameters in equations 2-4 are chosen based on the soil properties shown in Tables 1 and 2.

G_0 obtained for soil layers tested are reasonably in good agreement with the G_0 evaluated from the literature methods. For further analysis, G_0 at a depth of $4d$~$5d$ above and below the interface are considered as average G_0 for the clay and sand layers respectively. This will result in an average G_0 of 23 MPa for the clay layer, and, as not many data points are available in the sand layer, an average G_0 of 184 MPa that fits in between the literature methods (Oztoprak & Bolton, 2013 and Hardin & Drnevich, 1972) was considered for the sand layer. With the considered average G_0, there will be a stiffness contrast of eight between the clay and sand layers.

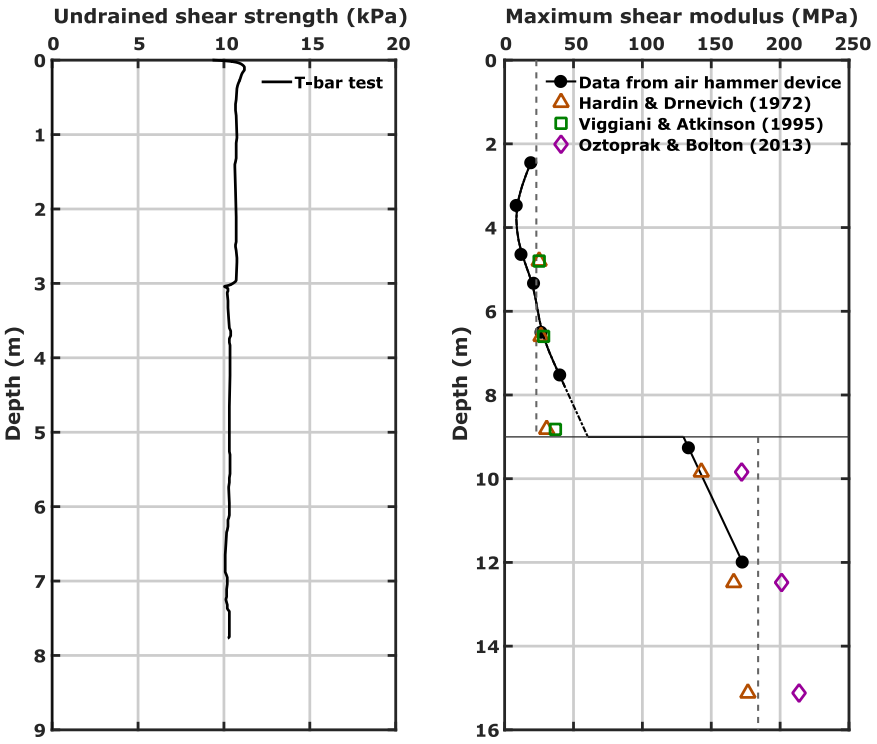

(a) (b)

Fig. 5. (a) Undrained shear strength of clay layer (b) maximum shear modulus of soil layers

DYNAMIC BEHAVIOUR OF SOIL STRATA AND PILE FOUNDATIONS

To determine the natural frequency of soil strata, scaled Kobe motion (BE5) was used as it consists of a wider range of frequencies in comparison to the simple sinusoidal excitations (see Fig. 4). Figure 6a shows the responses of BE5 excitation, far-field soil surface, single pile and pile group in terms of the amplitude of excitation against the frequency, obtained by using a fast Fourier transform (FFT). Figure 6b shows the normalised responses of far-field soil surface and pile foundations with respect to BE5 excitation. Clear peaks at 1.5 Hz and 1.7 Hz in Fig. 6b indicate that the natural frequency of the soil strata can be in between 1.5~1.7 Hz. Using the average small-strain shear modulus values for the top and bottom soil layers (see Fig. 5b), the natural frequency of soil strata was estimated approximately using equation 5 as 2.44 Hz.

$$f = \left(4\sum_{i=1}^{n}\left(\frac{h_i}{\sqrt{G_i/\rho_i}}\right)\right)^{-1} \qquad (5)$$

where, n is the number of soil layers and h_i is the thickness of each soil layer in stratified soil.

As larger intensity Kobe motion induces significant strains in the soil layers, the observed natural frequency is only between 1.5~1.7 Hz during BE5 excitation. Also, as shown in Figs. 6a and 6b, pile

foundations are forced to follow the soil movement and hence their peak responses are also observed at the natural frequency of the soil strata. However, the pile foundations' acceleration amplitude is slightly higher than the far-field soil surface due to the following two reasons: (i) pile-soil kinematic interaction induces relatively larger pile head displacements for free-head piles in comparison to the soil surface displacement, and (ii) the higher mass density of the pile material and corresponding inertial effects leads to higher accelerations in the pile foundations compared to the soil surface. Further, the single pile has higher acceleration amplitude than the pile group, probably due to the higher rotational stiffness of the pile group compared to single pile. It is also interesting to observe that the normalised amplitudes are less than one at higher frequencies (>2.5 Hz) in Fig. 6b for both soil surface and pile foundations. The soft clay layer is unable to transmit higher frequency components to surface and hence filtered out such frequencies. Pile foundations are vibrating at lower magnitudes of acceleration for such higher frequencies as the soil exhibits a smoothened response to high frequencies, and this is also a function of the intensity of the excitation. More details about the filtering effects in soft clay and corresponding pile foundations behaviour in such soils are discussed in Garala & Madabhushi (2019).

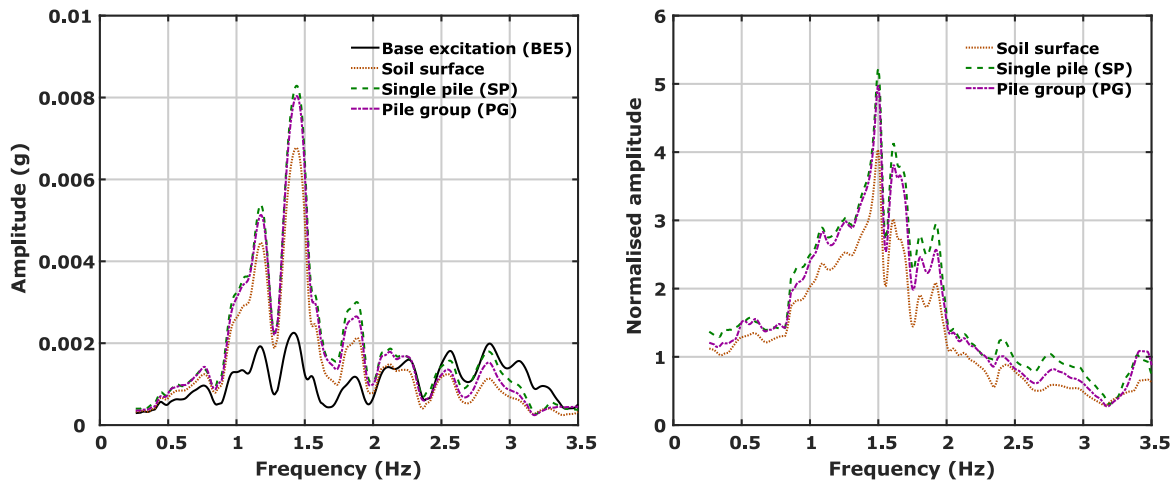

(a) (b)

Fig. 6. Acceleration response of soil and pile foundations (a) acceleration amplitude against the frequency (b) normalised acceleration amplitude against the frequency for the scaled Kobe motion (BE5)

Considering the shear waves propagation in a stratified soil, it is well established that as the seismic shear waves propagate from a stiffer layer to a softer layer, the wave amplitude will get amplified (Kramer, 1996). The shear wave amplification as it propagates from dense sand layer to the surface of the soft clay layer can be clearly seen in Fig. 7. Similar behaviour of soil amplification was observed in all excitations although only soil behaviour during BE1 and BE5 excitations are shown in Fig. 7. Table 4 lists the amplification ratios (ratio of peak surface acceleration to the peak base excitation acceleration) measured during different excitations. The peak soil amplification ratio is observed during BE2 excitation, probably due to its predominant excitation frequency (1.167 Hz) being close to the strain-dependent natural frequency of the soil strata. Table 4 also shows the acceleration amplification ratios of pile foundations tested, in which the single pile and pile group have a peak amplification ratio for BE2 excitation. Also, the single pile shows higher amplification ratio than the pile group for all excitations with the difference between the two increasing with the increase in intensity of the base excitation.

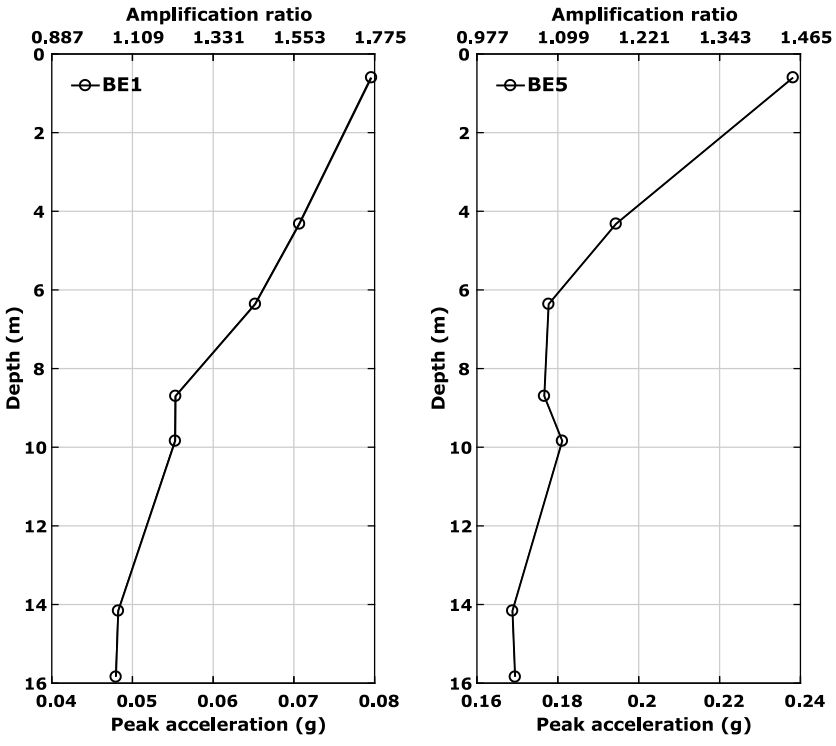

(a) (b)

Fig. 7. Peak acceleration at different depths in the soil model during (a) BE1 and (b) BE5 excitations

Table 4. Amplification ratios of soil strata and pile foundations

Excitation	Peak base acceleration (g)	Amplification ratio		
		Soil surface	Single pile	Pile group
BE1	0.045	1.78	1.98	1.96
BE2	0.087	2.07	2.60	2.56
BE3	0.174	1.36	1.75	1.65
BE4	0.193	1.59	2.37	2.16
BE5	0.164	1.45	2.07	1.93

KINEMATIC PILE BENDING MOMENT DURING EXCITATIONS

The kinematic pile bending moments (M_k) during different base excitations were measured using the strain gauges along the pile length at different locations for both single pile and end piles (P1 and P3) of the pile group (see Figs. 1 and 2). In this study, bending at pile tip is assumed to be zero for both single pile and end piles of the pile group. Figures 8-10 show the M_k measured in strain gauged piles at a specific instant of excitation, M_k when maximum M_k occurs and the envelope of maximum absolute M_k, respectively. In the same figures, pile bending is also represented using pile bending strain at the outer fiber, ε_p, as recommended by Mylonakis (2001).

It can be seen from Fig. 8 that the single pile and end piles of the pile group are responding in a similar manner at the same instant of excitation for all the excitations. However, Fig. 9 illustrates that the peak M_k occurs at different instants for single pile and end piles of the pile group based on the frequency and intensity of the excitation. Except for BE1 excitation, the time difference for peak M_k occurrence for single pile and end piles of the pile group is relatively small. Furthermore, for single pile and end piles of the pile group, peak M_k occurs close to the interface of soil layers as shown in Figs. 9 and 10. This is to be expected as there will be strain discontinuity at the interface due to sharp stiffness contrast between the soil layers. It is important to mention that no curve fitting techniques were employed to fit the bending moment data to allow for the continuity of the piles. Any such curve fitting may therefore result in slightly larger or smaller peaks in M_k and their location can be either at the

interface or slightly above/below the interface. However, Nikolaou et al. (1995) and Nikolaou et al. (2001) also observed the peak M_k at a depth ~1d above or beneath the interface for free-head single piles in their analytical approach based on the beam on dynamic Winkler foundation. Further, at the shallower depths, the peak M_k increases with the increase in intensity of the excitation for end piles of the pile group and exceeds the peak M_k of single pile during larger intensity excitations as shown in Fig. 10. This is probably due to the frame action in pile groups. Nevertheless, the peak M_k at shallower depths is always less than the peak M_k measured at the interface of soil layers for both single pile and end piles of the pile group (see Fig. 10). Also, as shown in Figs. 9 and 10, the M_k at a depth of 9.48 m is close to the M_k at 10.98 m for the end piles in pile group. This suggests that the peak bending moment occurs at a deeper location for the pile group compared to a single pile, which can be due to the soil confinement effects between the closely spaced piles in a group. Further, the peak M_k for end piles of the pile group is slightly less than that of a single pile as shown in Fig. 10. This difference increases with the increase in the intensity of the excitation, indicating that the piles in closely spaced pile group will always attract lower M_k than a single pile. Moreover, the difference between peak M_k of P1 and P3 of the pile group is also increasing with the increase in intensity of the excitation. This indicates that all piles of the pile group may not be subjected to the same M_k due to shadowing effects, which is very significant at larger intensity excitations. In this case, P1 always had larger M_k than P3, due to the bias in base excitations created by the first half-cycle. In a larger pile group in practice, some of the intermediate piles may see significantly smaller M_k relative to the leading-edge piles.

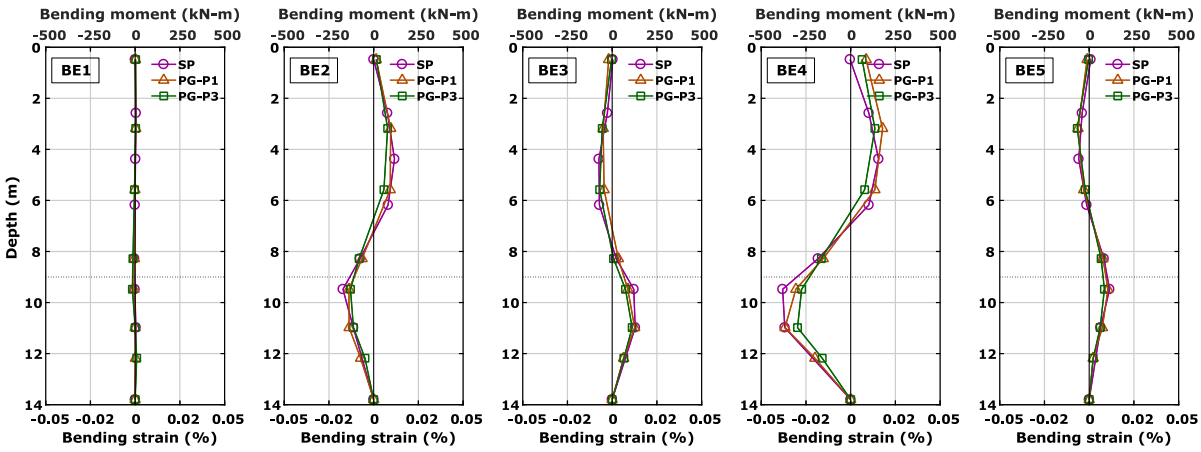

Fig. 8. Kinematic pile bending moments at the 8th second of excitation

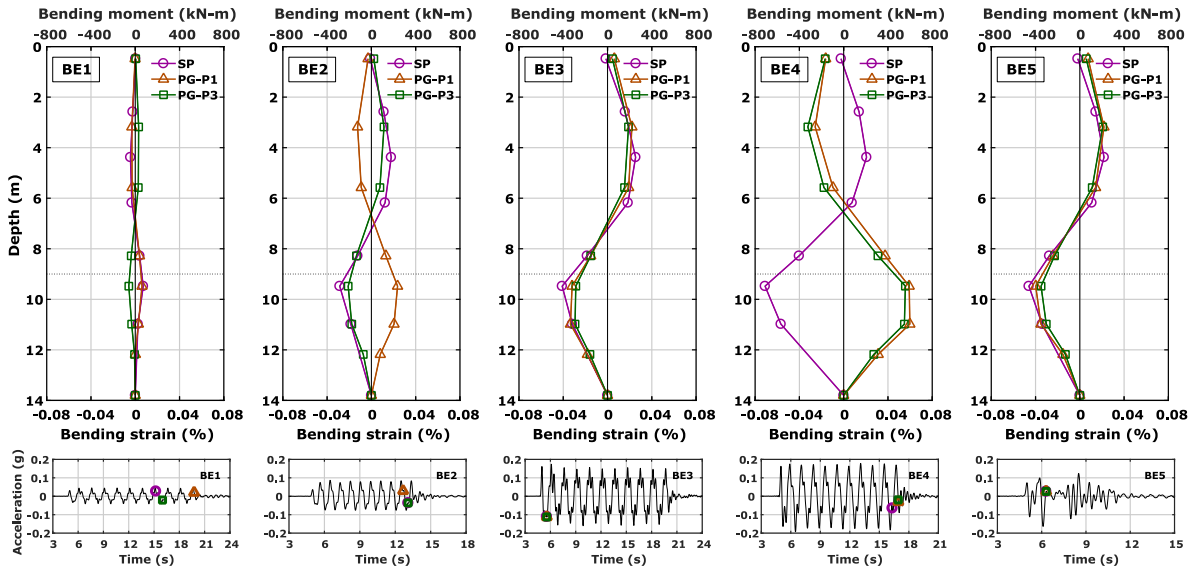

Fig. 9. Kinematic pile bending moments at the instant of maximum bending moment occurrence

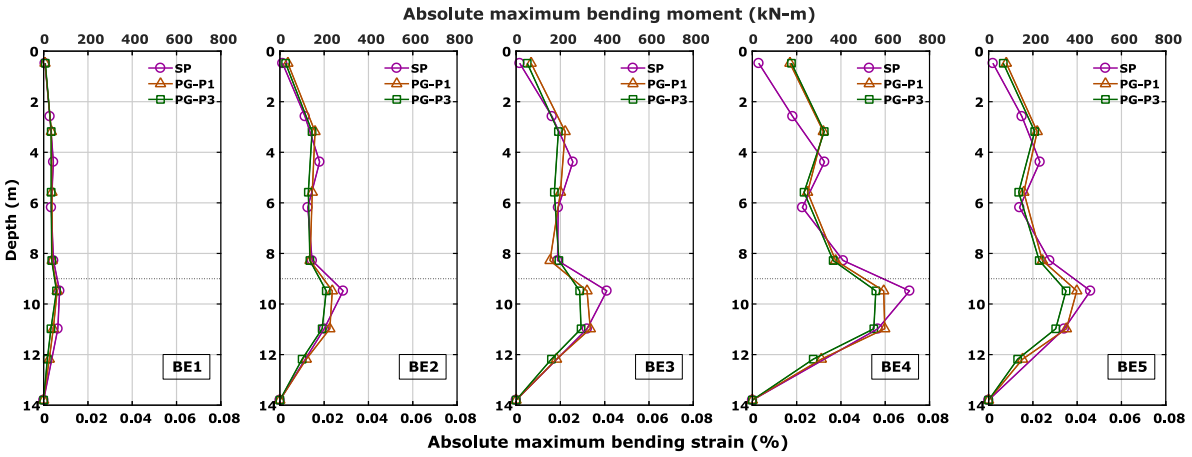

Fig. 10. Maximum absolute kinematic pile bending moment envelopes

Figure 11 shows the relationship between the peak pile acceleration and peak M_k. As there is no yielding or failure of pile foundations, a linear relationship is exhibited between the peak pile acceleration and peak M_k. As discussed earlier, Fig. 11 also depicts that the single pile has higher M_k than pile group and further in the pile group, P1 will be subjected to relatively larger M_k than P3 due to shadowing effects.

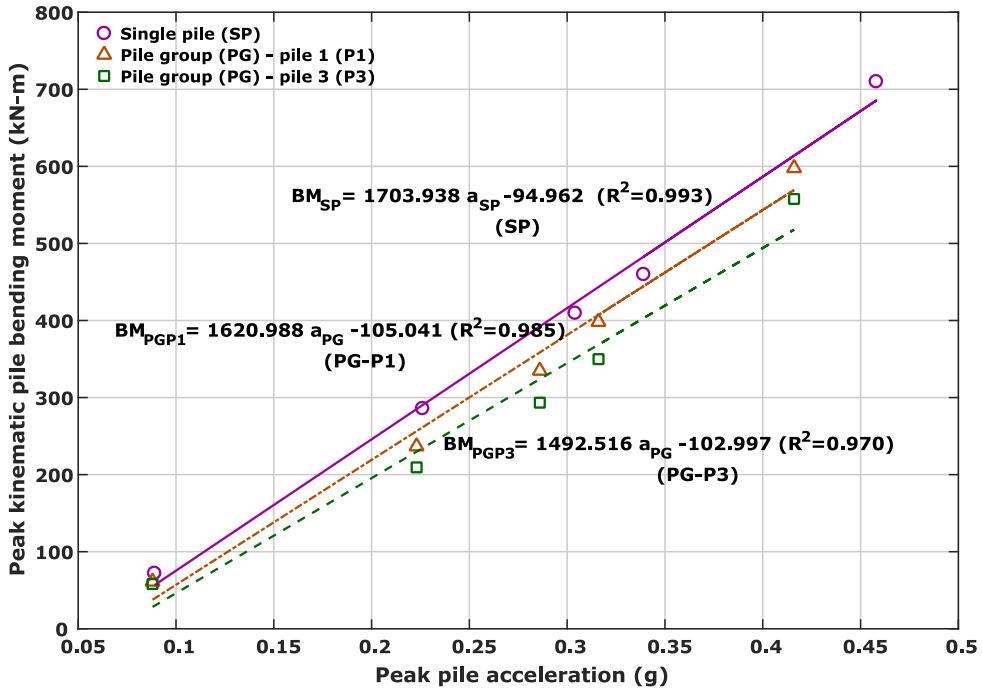

Fig. 11. Relationship between the peak pile acceleration and peak kinematic pile bending moment

Post-excitation kinematic pile bending moment

At the end of every excitation, the strain gauges measured a small residual M_k in both single pile and end piles of the pile group. Figure 12 shows the residual M_k measured by the pile foundations during all base excitations. From BE1 to BE4 excitations, as expected, the residual M_k increases with the increase in intensity of the excitation as shown in Fig. 12. Further, the end piles of the pile group have larger residual M_k than the single pile. Further in pile group, P3 shows higher residual M_k than the P1. This is opposite to the dynamic behaviour discussed in the earlier section. During the scaled Kobe motion (BE5), it is interesting to note that the residual M_k values are much smaller for all the piles. This may be due to the presence of only a few cycles of strong shaking in this motion compared to other base excitations (see Fig. 4). In Fig. 13, a sketch of the deformed end piles of the pile group after excitation is presented at an exaggerated scale showing the opposite curvatures in the leading and lagging piles. It must be noted that these residual bending moments were not considered earlier (i.e., in Figs. 8 to 11).

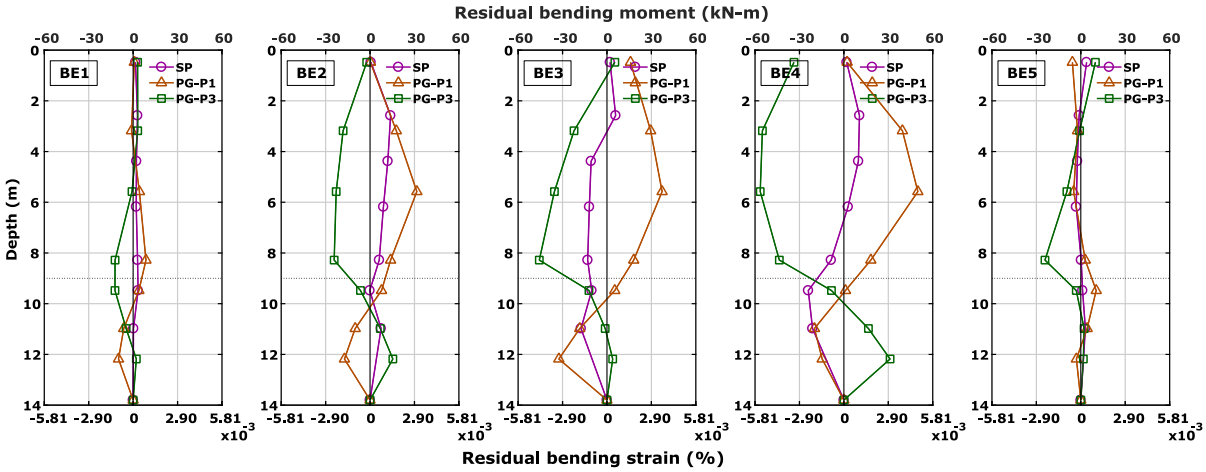

Fig. 12. Post-excitation (residual) kinematic pile bending moments

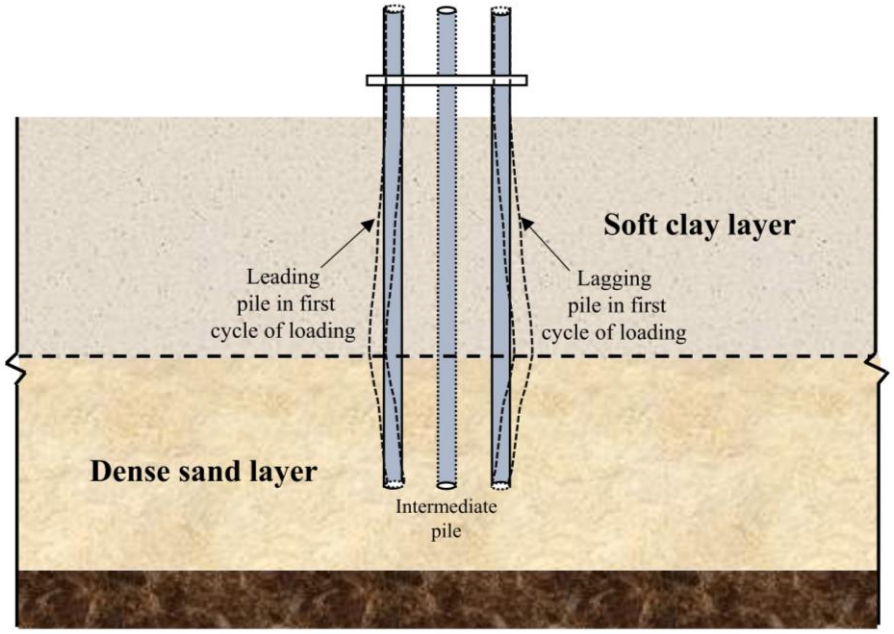

Fig. 13. A sketch of post-excitation deformed end piles of the pile group at an exaggerated scale

COMPARISON WITH LITERATURE METHODS

Several simplified procedures and analytical solutions have been proposed for the evaluation of kinematic pile bending moments (M_k) during earthquakes. Early attempts of Margason & Halloway (1977) for determining M_k is based on the free-field soil curvatures using finite difference approach, assuming that the pile follows the surrounding soil motion during earthquakes. Despite its simplicity, the method showed satisfactory performance in predicting the pile head moment in homogeneous or two-layer soils if the interface is deep enough (de Sanctis et al., 2010; Di Laora et al., 2013). However,

this method is not useful for a layered soil profile with sharp stiffness contrast between the layers and consequent different shear strains above and below the interface. Table 5 lists some of the equations available in the literature to compute the peak M_k at the interface of two-layered soils during the earthquakes. The methods that do not require any ground response analysis are only considered here as these are widely used in geotechnical practice.

Dobry & O'Rourke (1983) proposed an analytical equation as shown in Table 5. They assumed a uniform static shear stress field in the soil mass that generates constant shear strain within each layer. This method considers the stiffness contrast between the soil layers and soil-pile interaction, nevertheless, the thickness of soil layers and excitation frequency effects are not included in this method. Nikolaou et al. (1995) proposed an equation using beam on dynamic Winkler foundation concept with frequency-dependent springs and dashpots accounting for soil stiffness and radiation damping respectively. Based on extensive regression analysis, an equation was proposed to determine the steady-state maximum kinematic pile bending moment (M_{max}) as shown in Table 5. The peak M_k generated by the actual ground motion (i.e., for transient conditions) is determined by multiplying the M_{max} with a reduction factor η_1. η_1 is a function of excitation frequency and number of loading cycles and varies from 0.2 to 0.5. The value of the reduction factor η_1 is chosen based on the proximity of the excitation frequency to the natural frequency of the soil strata with η_1 close to 0.2 if the excitation frequency is far from the natural frequency of the soil strata. Mylonakis (2001) proposed an equation (see Table 5) considering the effects of thickness of the soil layers, dynamic nature of excitation and soil damping. The frequency effects are incorporated using an amplification factor (φ). The factor φ can exceed 2 for stiff piles (E_p/E_1 =10000) and deep interfaces (h_1/d=20), where E_p and E_1 are Young's moduli of the pile and top soil layer respectively and, h_1 and d are the thickness of top soil layer and pile diameter respectively. For softer piles (E_p/E_1 < 1000) and for the range of seismic frequencies of interest, φ is usually less than 1.25. Later, Nikolaou et al. (2001) proposed an equation for determining the harmonic steady-state kinematic pile bending moment under resonant conditions (M_R) as shown in Table 5. This equation is based on the characteristic shear stress (τ_c), which is a function of maximum free-field surface acceleration (a_s). The peak M_k for transient seismic excitations is smaller than the M_R

determined from Nikolaou et al. (2001) and a reduction factor (η_2) was proposed similar to Nikolaou et al. (1995). Equations (6) and (7) are provided to determine η_2 as a function of the number of loading cycles (N_c).

$$\eta_2 \approx 0.04N_c + 0.23 \text{ (for resonant conditions)} \quad (6)$$

$$\eta_2 \approx 0.015N_c + 0.17 > 0.2 \text{ (for non-resonant conditions)} \quad (7)$$

Maiorano et al. (2009) proposed correction coefficients for the formulae proposed by Mylonakis (2001) and Nikolaou et al. (2001) by performing extensive finite element analyses. Recently, Di Laora et al. (2012) performed rigorous three-dimensional dynamic finite element analyses for various pile-soil configurations and proposed a simplified formula which employs the maximum transient shear strain at the interface as shown in Table 5.

The literature methods shown in Table 5 are developed for single pile foundations assuming both soil and pile will behave as either linear elastic materials or equivalent linear visco-elastic materials. Hence, their performance in estimating the peak M_k for large intensity earthquakes is questionable due to the high soil non-linearity induced under such intense earthquakes. To evaluate, the average initial shear moduli of 23 MPa and 184 MPa were considered for the top soft clay and bottom dense sand layers respectively (see Fig. 5b). The equivalent prototype pile dimensions, 0.666 m diameter solid concrete pile with a flexural rigidity of 344 MNm^2, were used in the computations as most of the methods in the literature are applicable only for the solid cylindrical piles. The peak accelerations measured close to the far-field clay surface were used in computing the τ_c and peak shear strain (γ_1) in the clay layer. A η_1 of 0.2 was used while computing the peak M_k from Nikolaou et al. (1995) and no reduction factor was used for Nikolaou et al. (2001), for reasons being explained later in this section. A φ of 1.25 was used for computing the peak M_k from Mylonakis (2001). Figure 14 shows the comparison of the experimental and the predictions by the methods outlined in Table 5. It is clear that most of these methods are under-estimating the peak M_k in comparison to the experimentally determined values. Within the literature methods, the predictions for BE1 excitation which satisfies the linear elastic or visco-elastic assumption, Nikolaou et al. (1995) results in a closer estimation compared to the Nikolaou

et al. (2001), which gives a peak M_k very far from the experimental value. Moreover, the peak M_k obtained by Nikolaou et al. (2001) is not reduced for the transient seismic conditions. Therefore, the peak M_k will be much lower if the computed peak M_k from Nikolaou et al. (2001) is reduced by a factor η_2 to consider the frequency effects. As Fig. 14 shows, the equations of Mylonakis (2001) and Di Laora et al. (2012) can result in an acceptable peak M_k for the smaller intensity excitations. Further, as shown in Fig. 14, the difference between experimentally determined peak M_k and literature methods increases with the increase in intensity of the excitation and literature methods severely under-estimate the peak M_k at larger intensity excitations, including Nikolaou et al. (1995). Considering higher η_1 (up to 0.5) can result in a better estimation of peak M_k from Nikolaou et al. (1995) at larger intensity excitations, but this will lead to large over-estimation of peak M_k at smaller intensity excitations.

Table 5. Methods to compute the kinematic pile bending moment

Study	Method	Equation
Dobry & O'Rourke (1983)	Analytical solution using the beam on Winkler foundation	$M_k = 1.86\left(E_p I_p\right)^{0.75}(G_1)^{0.25}\gamma_1 F$ $F = \frac{(1-c^{-4})(1+c^3)}{(1+c)(c^{-1}+1+c+c^2)};\ c = \left(\frac{G_2}{G_1}\right)^{0.25}$ $\gamma_1 = \frac{r_d \rho_1 h_1 a_s}{G_1};\ r_d = r_d(z) \cong 1 - 0.015z$
Nikolaou et al. (1995)	Regression analysis using the beam on dynamic Winkler foundation	$M_{max} = \frac{2.7}{10^7} E_p d^3 \left(\frac{a_{rock}}{g}\right)\left(\frac{L}{d}\right)^{1.30}\left(\frac{E_p}{E_1}\right)^{0.7}\left(\frac{V_2}{V_1}\right)^{0.3}\left(\frac{h_1}{L}\right)^{1.25}$ $M_k = \eta_1 M_{max}$
Mylonakis (2001)	Analytical solution using the beam on dynamic Winkler foundation	$M_k = \left(E_p I_p\right)\left(\frac{\varepsilon_p}{\gamma_1}\right)_{\omega=0}\gamma_1\left(\frac{\varphi}{r}\right)$ $\left(\frac{\varepsilon_p}{\gamma_1}\right)_{\omega=0} = \frac{(c^2-c+1)\left\{\left[3\left(\frac{k_1}{E_p}\right)^{0.25}\left(\frac{h_1}{d}\right)-1\right]c(c-1)-1\right\}}{2c^4\left(\frac{h_1}{d}\right)}$ [Minimum value of $\left(\frac{\varepsilon_p}{\gamma_1}\right)$ is 0.05]

		$\gamma_1 = \frac{r_d \rho_1 h_1 a_s}{G_1}$; $r_d = r_d(z) \cong 1 - 0.015z$
		$\varphi \cong 1 \sim 1.25$; $c = \left(\frac{G_2}{G_1}\right)^{0.25}$
		$k_1 = \frac{3E_1}{1-\vartheta^2}\left(\frac{E_p}{E_1}\right)^{-1/8}\left(\frac{L}{d}\right)^{1/8}\left(\frac{h_1}{h_2}\right)^{1/12}\left(\frac{G_2}{G_1}\right)^{-1/30}$
Nikolaou et al. (2001)	Regression analysis using the beam on dynamic Winkler foundation	$M_R = 0.042\,\tau_c d^3\left(\frac{L}{d}\right)^{0.30}\left(\frac{E_p}{E_1}\right)^{0.65}\left(\frac{V_2}{V_1}\right)^{0.50}$
		$\tau_c \approx a_s \rho_1 h_1$; $M_k = \eta_2 M_R$
Di Laora et al. (2012)	Regression analysis using three-dimensional finite element analyses	$M_k = \frac{2E_p I_p}{d}\left(\frac{\varepsilon_p}{\gamma_1}\right)\gamma_{1,d}$
		$\left(\frac{\varepsilon_p}{\gamma_1}\right) = \chi\left[-0.5\left(\frac{h_1}{d}\right)^{-1} + \left(\frac{E_p}{E_1}\right)^{-0.25}(c-1)^{0.5}\right]$
		$c = \left(\frac{G_2}{G_1}\right)^{0.25}$; $\gamma_{1,\mathrm{d}} = \frac{\rho_1 h_1 a_s}{G_1}$; $\chi \cong 0.93$
Misirlis et al. (2019a, b)	Three-dimensional finite element analyses	$\frac{M_k}{\rho_1 g h_1 d^3} = e^{-4.49}\left(\frac{a_s}{g}\right)^{1.02}\left(\frac{L}{d}\right)^{0.46}\left(\frac{E_p}{E_1}\right)^{0.94}\left(\frac{V_2}{V_1}\right)^{-0.26}\left(\frac{h_1}{L}\right)^{0.018}\left(\frac{T_i}{T_s}\right)^{1.16} N^{0.25}$

a_{rock} and a_s are accelerations at the bed-rock level and soil surface respectively; d is pile diameter; E_p, E_1 and E_2 are Young's moduli of the pile, top and bottom soil layers respectively; G_1 and G_2 are shear moduli of top and bottom soil layers respectively; $h_1$and h_2 are thicknesses of the top and bottom layers respectively; I_p is the cross-sectional moment of inertia of pile; k_1 is spring coefficient; L is length of the pile embedded in soil; M_k is kinematic pile bending moment; M_{max} is steady-state maximum kinematic pile bending moment; M_R is harmonic steady-state pile bending moment under resonance conditions; N is number of uniform cycles of the sinusoidal base excitation; r is radius of the pile; T_i and T_s are mean period of the input motion and first fundamental period of soil profile assuming elastic behaviour; V_1 and V_2 are shear wave velocities of the top and bottom soil layers respectively; z is depth from the ground surface; r_d is depth factor; $\gamma_1$and $\gamma_{1,d}$ are shear strains in the top layer of the soil; ϑ is Poisson's ratio of top soil layer; ε_p is pile bending strain; $\eta_1$and η_2 are reduction factors; ρ_1 is mass density of the top soil layer; τ_c is characteristic shear stress in top soil layer; φ is frequency factor; χ is regression coefficient; ω is angular frequency.

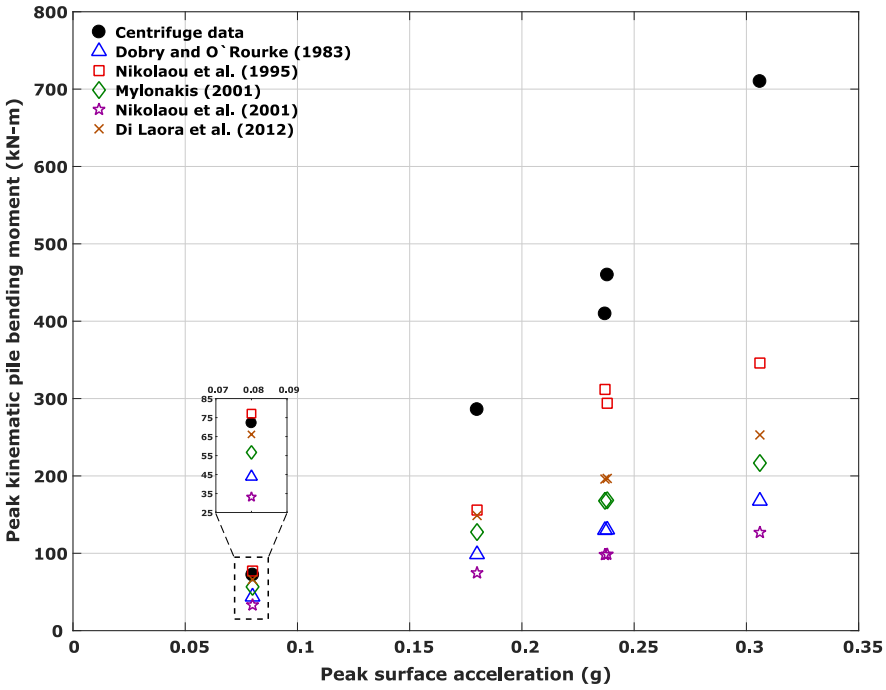

Fig. 14. Comparison of experimental kinematic pile bending moments with literature methods

IMPROVEMENTS TO LITERATURE METHODS BY INCLUSION OF SOIL NON-LINEARITY

From Fig. 14, it is clear that considering the initial shear moduli for soil layers will result in significant under-estimation of peak M_k as these methods fail to capture the sharp change in strains due to stiffness contrast between the soil layers during large intensity earthquakes. An attempt is made to improve the performance of these methods by considering the soil non-linearity under such intense earthquakes. In this section, the mobilised shear moduli were considered for the top and bottom soil layers by computing the shear stresses and strains from the actual soil accelerations measured in the experiment following Brennan et al. (2005). Medium to larger intensity sinusoidal excitations (BE2 to BE4) were only considered for computing the shear modulus degradation curves. Figures 15-18 show the normalised shear modulus (G/G_o) degradation curves determined at different depths of interest in this study. Figures 15-18 are plotted considering all loading cycles in excitations BE2 to BE4 and the closed symbol in each excitation represents the load cycle at which the peak M_k was observed for the single pile (see Fig. 9). To compute the peak M_k from the literature methods, the mobilised shear moduli during BE2 to BE4 in the clay layer were determined from Fig. 15, at a depth close to where the initial

average shear modulus (G_1) was considered for the clay layer. However, due to the non-availability of mobilised shear moduli at the required depth of interest in the sand layer, average shear moduli were taken using shear moduli computed at a depth of 9.84 m (Fig. 17) and 14.16 m (Fig. 18). The shear strain in the clay layer (γ_1) close to the interface for various excitations was determined from Fig. 16 rather than computing it from the soil surface acceleration. Figure 19 shows the comparison between the experimentally determined peak M_k and those determined from the literature methods for BE2 to BE4 excitations. As can be seen in Fig. 19, some of the literature methods predict M_k close to the experimentally determined peak M_k, even for larger intensity excitations. Among the methods considered, Di Laora et al. (2012) results in a reasonable estimation, followed by Mylonakis (2001) and Dobry & O'Rourke (1983). However, Nikolaou et al. (1995) over-estimates and Nikolaou et al. (2001) under-estimates the peak M_k, both by large extents. It is important to highlight that many of the methods in Table 5 assume a linear variation of strain with depth and use the soil surface accelerations to estimate the shear strains at the interface. In this section, the shear strains at the interface are determined from the experimentally measured acceleration time-histories and are not based on the soil surface accelerations. The improvements obtained in the prediction of peak M_k seen in Fig. 19, suggest that in practice a proper ground response analysis is required to determine the shear strain at the interface and the degradation in the shear moduli proportional to the strains in each of the layer must be allowed for.

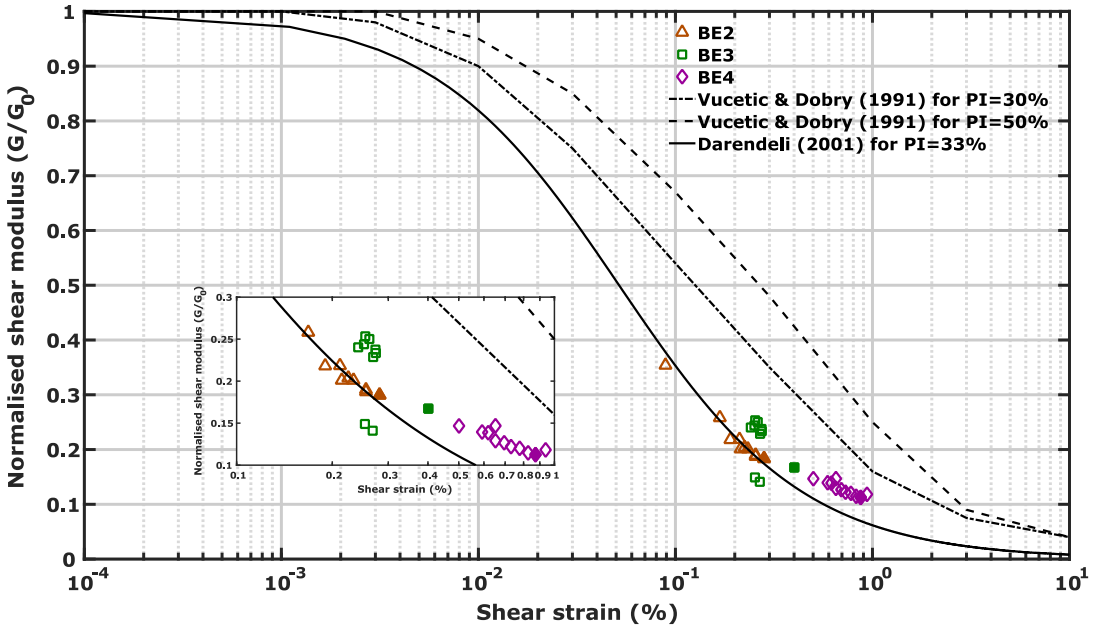

Fig. 15. Shear modulus degradation curve at a depth of 6.9 m

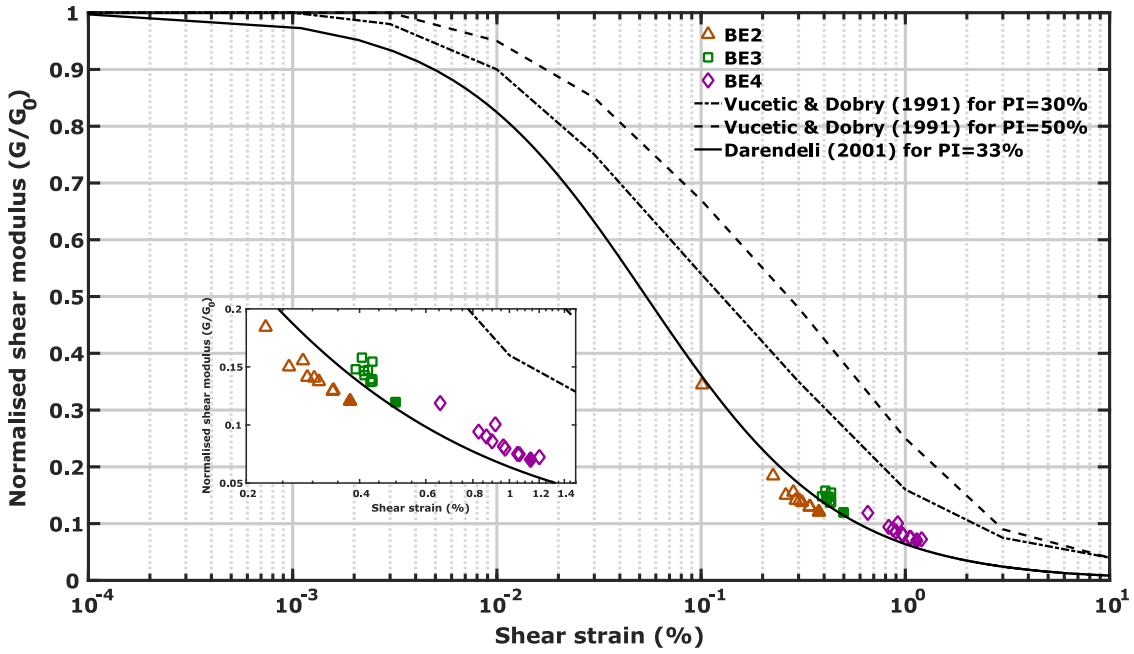

Fig. 16. Shear modulus degradation curve at a depth of 8.7 m

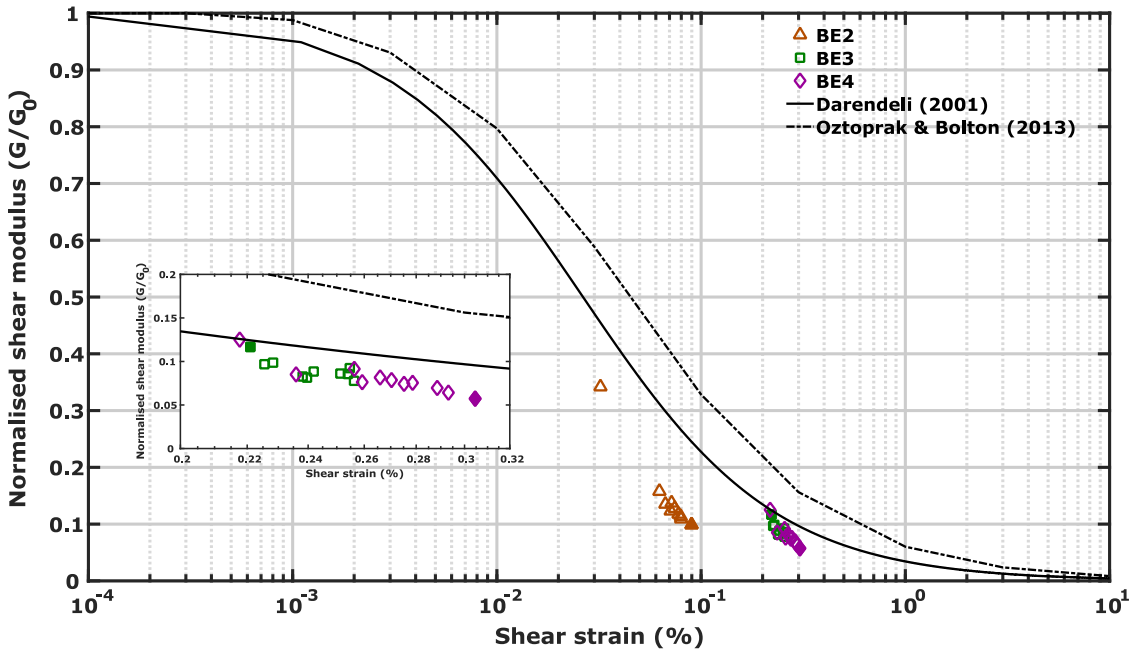

Fig. 17. Shear modulus degradation curve at a depth of 9.84 m

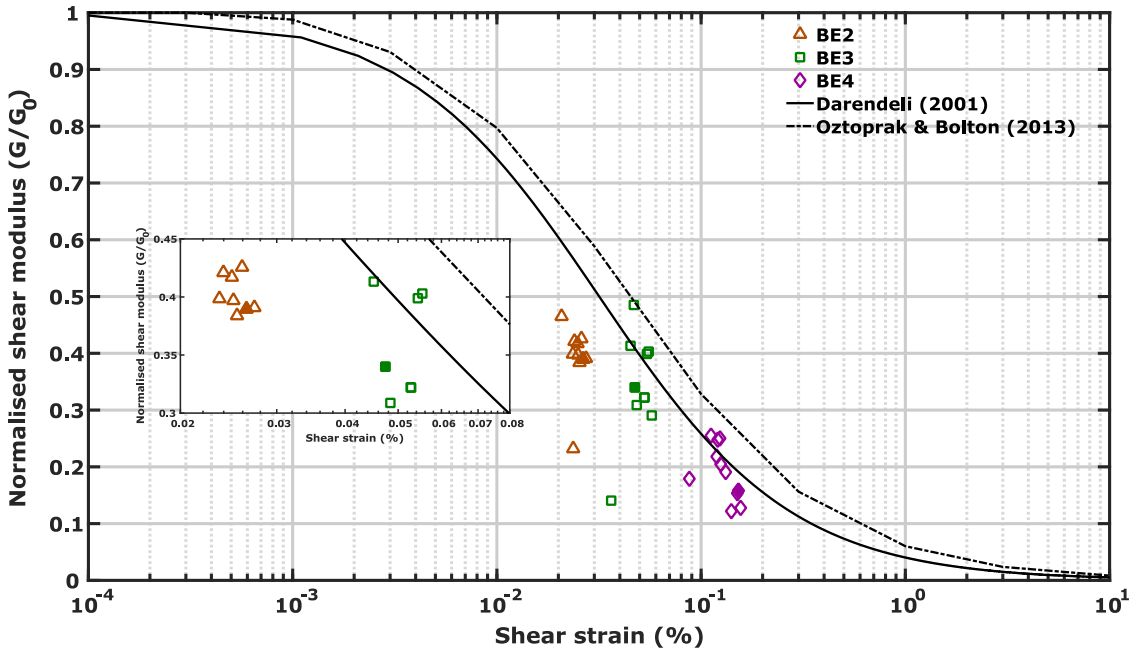

Fig. 18. Shear modulus degradation curve at a depth of 14.16 m

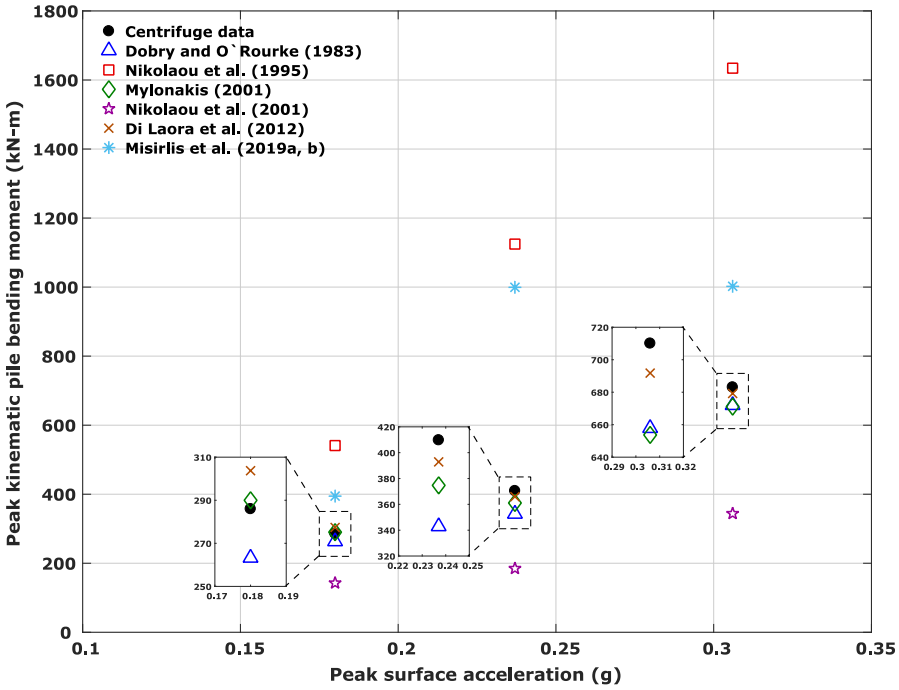

Fig. 19. Comparison of experimental kinematic pile bending moments with literature methods considering soil non-linearity

Recently, Misirlis et al. (2019a, b) proposed another equation as shown in Table 5 for determining the peak M_k at the interface of two soil layers by considering the soil non-linearity effects in their three-dimensional finite element analyses using PLAXIS. While computing the peak M_k following Misirlis

et al. (2019a, b), the maximum shear moduli and shear wave velocities measured directly in the experiments (see Fig. 5b) were used as recommended by the authors. This is reasonable as the PLAXIS analysis takes into account the soil non-linear effects via the Hardening Soil model with small-strain stiffness (HSsmall) used in their study. Further, the first fundamental period of the soil profile (T_s) was taken as 0.41 seconds and 10 uniform sinusoidal loading cycles (N) with the mean period of input motion (T_i) as shown in Fig. 4 were considered for BE2 to BE4 excitations. Figure 19 includes the comparison of Misirlis et al. (2019a, b) with the centrifuge data. It is seen that for the three excitations considered here, Misirlis et al. (2019a, b) overestimates the peak M_k significantly even for moderate intensity excitations and differences are much bigger for larger intensity excitations. However, it must be noted that Misirlis et al. (2019a, b) equation was based on PLAXIS analyses with loose and medium dense, dry granular soil layers and ignored any soil dilation, although their equation depends only on the ratio of shear wave velocities (see Table 5) to include the stiffness contrast. Therefore, the application of Misirlis et al. (2019a, b) equation to any soil type other than the intended loose to medium dense, dry cohesionless soils can result in an unrealistic estimation of peak M_k as shown in Fig. 19.

CONCLUSIONS

A series of dynamic centrifuge experiments were performed at 60g to investigate the influence of kinematic loads on a single pile (SP) and closely spaced 3×1 row pile group (PG) embedded in a two-layer soil during the earthquakes. The soil model consisted of a soft clay layer overlying the dense sand. Undrained shear strength of the clay and stiffness of soil layers were evaluated using the T-bar tests and air hammer device respectively. Various base excitations ranging from smaller intensity to larger intensity sinusoidal excitations along with a scaled 1995 Kobe earthquake motion were considered. The following are the major conclusions of the study:

- As expected, a linear relationship was observed between the peak pile acceleration and peak kinematic pile bending moment (M_k) in both single pile and pile group. The peak M_k was observed at a depth slightly beneath the interface of the soil layers for both single pile and pile group irrespective of intensity of the excitation. However, this depth is slightly larger for pile group compared to the single pile.

- The piles of the pile group will attract smaller M_k than a single pile. However, the post-seismic residual kinematic bending moments are bigger for the piles in a group than the single pile. These residual moments increase with the increase in intensity of the excitation. In addition, the end piles of the pile group have different peak M_k and residual bending moments highlighting the pile group shadowing effects.
- Using the initial shear moduli for larger intensity excitations will result in under-estimating the peak M_k from literature methods as they fail to consider the sharp stiffness contrast or consequent shear strain variation between the soil layers. As a result, the difference between experimental peak M_k and literature methods increases with the increase in intensity of the excitation, highlighting the inadequacy of the current literature methods for large intensity excitations (see Fig. 14).
- The predictions of the literature methods can be improved by considering strain mobilisation during large earthquakes. Using the mobilised shear moduli of soil layers and accurate shear strain at the interface, some methods in the literature (see Fig. 19) were shown to give reasonable estimates of the peak M_k even for large intensity excitations.

It must be pointed out that this study was limited in terms of pile stiffnesses and soil profiles considered. A wider study looking at these variables can help strengthen the observations made in this paper.

ACKNOWLEDGEMENTS

The authors would like to thank Prof. Giulia Viggiani, Dr Stuart Haigh and Prof. Luca de Sanctis for their technical discussions. The first author would also like to thank the Commonwealth Scholarship Commission (CSC) and Cambridge Trust for their doctoral scholarship. The authors also extend their appreciation to the technicians at the Schofield Centre of Cambridge University for their assistance during the centrifuge experiments.

NOTATION

a_g design ground acceleration

a_{rock} accelerations at the bed-rock level

a_s accelerations at the soil surface

BE	base excitation
c_u	undrained shear strength of clay
d	pile diameter
e	void ratio of soil
E_1, E_2	Young's moduli of top and bottom soil layers
E_p	Young's moduli of pile
G_0	Maximum shear modulus of soil
G_1, G_2	shear moduli of top and bottom soil layers
h_1, h_2	thicknesses of the top and bottom layers
I_p	cross-sectional moment of inertia of pile
k_1	spring coefficient
L	length of the pile embedded in soil
M_k	kinematic pile bending moment
M_{max}	steady-state maximum kinematic pile bending moment
M_R	harmonic steady-state kinematic pile bending moment under resonance conditions
N	number of uniform cycles of the sinusoidal base excitation
OCR	over-consolidation ratio
p'	mean effective stress
p_r, p_{ref}	reference pressures of 1 kPa and 100 kPa
PG	pile group
PI	plasticity index of clay
r	radius of the pile
S	soil factor
SP	single pile
T_i, T_s	mean period of the input motion and first fundamental period of the soil profile
v_s	shear wave velocity of soil layer
V_1, V_2	shear wave velocities of the top and bottom soil layers respectively
z	depth from the ground surface
r_d	depth factor
$\gamma_1, \gamma_{1,d}$	shear strains in the top layer of the soil

ε_p pile bending strain

η_1, η_2 reduction factors for Nikolaou et al. (1995) and Nikolaou et al. (2001)

ρ_1 mass density of the top soil layer

τ_c characteristic shear stress

ρ mass density of the soil layer

φ frequency factor

χ regression coefficient

ω angular frequency

ϑ Poisson's ratio of top layer

REFERENCES

ASTM D4253 (2016). Standard test methods for maximum index density and unit weight of soils using a vibratory table. *ASTM International*, West Conshohocken, PA.

ASTM D4254 (2016). Standard test methods for minimum index density and unit weight of soils and calculation of relative density. *ASTM International*, West Conshohocken, PA.

ASTM D6913 (2017). Standard test methods for particle-size distribution (gradation) of soils using sieve analysis. *ASTM International*, West Conshohocken, PA.

ASTM D7181 (2011). Standard method for consolidated drained triaxial compression test for soils. *ASTM International*, West Conshohocken, PA.

ASTM D854 (2014). Standard test methods for specific gravity of soil solids by water pycnometer. *ASTM International*, West Conshohocken, PA.

Brandenberg, S.J., Boulanger, R.W., Kutter, B.L. & Chang, D. (2005). Behaviour of pile foundations in laterally spreading ground during centrifuge tests. *Journal of Geotech. and Geoenviron. Eng.* **131**, No. 11, 1378-1391.

Brennan, A.J. & Madabhushi, S.P.G. (2002). Design and performance of a new deep model container for dynamic centrifuge testing. *Proc. International Conference on Physical Modelling in Geotechnics, Balkema, Rotterdam*, 183-188.

Brennan, A.J., Thusyanthan, N.I. & Madabhushi, S.P.G. (2005). Evaluation of shear modulus and damping in dynamic centrifuge tests. *Journal of Geotech. and Geoenviron. Eng.* **131**, No. 12, 1488–1498.

BS 8004 (2015). Code of practice for foundations. *British Standards Institution*, London, UK.

Darendeli, M.B. (2001). *Development of a new family of modulus reduction and material damping curves*. PhD Dissertation, University of Texas Austin.

de Sanctis, L. & Di Laora, R. (2017). Importance of kinematic interaction in the seismic vulnerability assessment of pile-supported buildings. *Rivista Italiana di Geotecnica* **51**, No. 4, 47-59.

de Sanctis, L., Maiorano, R.M.S. & Aversa, S. (2010). A method for assessing kinematic bending moments at the pile head. *Earthquake Engineering and Structural Dynamics* **39**, No. 10, 1133-1154.

Dezi, F., Carbonari, S. & Leoni, G. (2008). Kinematic interaction in pile foundations. *Proc. 14th World Conference on Earthquake Engineering*, Beijing, China.

Di Laora, R., Mandolini, A. & Mylonakis, G. (2012). Insight on kinematic bending of flexible piles in layered soil. *Soil Dynamics and Earthquake Engineering* **43**, 309-322.

Di Laora, R., Mylonakis, G. & Mandolini, A. (2013). Pile-head kinematic bending in layered soil. *Earthquake Engineering and Structural Dynamics* **42**, No. 3, 319-337.

Dobry, R. & O'Rourke, M.J. 1983. Discussion of 'Seismic response of end-bearing piles' by Flores Berrones, R. & Whitman, R.V. *Journal of Geotechnical Engineering* **109**, No. 5, 778-781.

EN 1998-5 (2004): Eurocode 8: Design of structures for earthquake resistance – Part 5: Foundations, retaining structures and geotechnical aspects. *CEN European Committee for Standardization* (CEN/TC250).

Fan, K., Gazetas, G., Kaynia, A. & Kausal, E. (1991). Kinematic seismic response of single piles and pile groups. *Journal of Geotech Eng.* **117**, No. 12, 1860–1879.

Garala, T.K. & Madabhushi, S.P.G. (2019). Seismic behaviour of soft clay and its influence on the response of friction pile foundations. *Bulletin of Earthquake Engineering* **17**, No. 4, 1919-1939.

Gazetas, G. & Mylonakis, G. (1998). Seismic soil-structure interaction: new evidence and emerging issues. *Proc. Geotechnical Earthquake Engineering and Soil Dynamics III, Geo-Institute ASCE Conference, Seattle*, Vol. II, 1119-1174.

Gazetas, G., Tazoh, T., Shimizu, K. & Fan, K. (1993). Seismic response of the pile foundation of Ohba-Ohashi Bridge. *Proc. 3rd International conference on Case Histories in Geotechnical Engineering, Missouri*, 1803-1809.

Ghosh, B. & Madabhushi, S.P.G. (2002). An efficient tool for measuring shear wave velocity in the centrifuge. *Proc. International Conference on Physical Modelling in Geotechnics, Balkema, Rotterdam*, 119–124.

Haigh, S.K. (2002). *Effects of liquefication on pile foundations in sloping ground*. PhD Dissertation, University of Cambridge, UK.

Hardin, B.O. & Drnevich, V.P. (1972). Shear modulus and damping in soils: Design equation and curves. *Journal of Soil Mechanics and Foundation Engineering Division* **98**, No. SM7, 667-692.

Haskell, J.J.M. (2013). *Guidance for the design of pile groups in laterally spreading soil*. PhD Dissertation, University of Cambridge, UK.

Kramer, S.L. (1996). *Geotechnical earthquake engineering*. Upper Saddle River, N.J., Prentice Hall.

Lau, B.H. (2015). *Cyclic behaviour of monopile foundations for offshore wind turbines in clay*. PhD Dissertation, University of Cambridge, UK.

Madabhushi, S.P.G. (2014). *Centrifuge modelling for civil engineers*. CRC Press, Taylor & Francis Group, Florida.

Madabhushi, S.P.G., Haigh, S.K. & Houghton, N.E. (2006). A new automated sand pourer for model preparation at University of Cambridge. *Proc. International Conference on Physical Modelling in Geotechnics, Hong Kong*, 217-222.

Madabhushi, S.P.G., Haigh, S.K., Houghton, N.E. & Gould, E. (2012). Development of a servo-hydraulic earthquake actuator for the Cambridge Turner beam centrifuge. *International Journal of Physical Modelling in Geotechnics* **12**. No. 2, 77-88.

Madabhushi, S.P.G., Knappett, J. & Haigh, S.K. (2010). *Design of pile foundations in liquefiable soils*. Imperial college press, London.

Maiorano, R.M.S., de Sanctis, L., Aversa, S. & Mandolini, A. (2009). Kinematic response analysis of piled foundations under seismic excitations. *Canadian Geotechnical Journal* **46**, No. 5, 571-584.

Margason, E. & Halloway, D.M. (1977). Pile bending during earthquakes. *Proc. Sixth World Conference on Earthquake Engineering, Meerut, India*, Vol. II, 1690-1696.

Misirlis, P., Anthi, M., Gerolymos, N. & Gazetas, G. (2019a). Pile-soil kinematic interaction considering soil nonlinearity and group effects. *Proc. Seventh International Conference on Earthquake Geotechnical Engineering, Rome, Italy*, 3966-3972.

Misirlis, P., Anthi, M., Gerolymos, N. & Gazetas, G. (2019b). Seismic pile-soil kinematic interaction with emphasis on soil nonlinearity and group effects. *Proc. Second International Conference on Natural Hazards and Infrastructure, Chania, Greece*.

Mizuno, H. (1985). Pile damage during earthquakes in Japan (1923-1983). *Dynamic response of pile foundations – Experiment, analysis and observation, ASCE Geotechnical Publication*, No. 11, 53-78.

Mucciacciaro, M. & Sica, S. (2018). Nonlinear soil and pile behaviour on kinematic bending response of flexible piles. *Soil dynamics and earthquake engineering* **107**, 195-213.

Mylonakis, G. 2001. Simplified method for seismic pile bending at soil-layer interfaces. *Soils and Foundations* **41**, No. 4, 47-58.

Nikolaou, A., Mylonakis, G. & Gazetas, G. (1995). *Kinematic bending moments in seismically stressed piles*. Report. NCEER-95-0022, National Center for Earthquake Engineering Research, State University of New York, Buffalo.

Nikolaou, S., Mylonakis, G., Gazetas, G. & Tazoh, T. (2001). Kinematic pile bending during earthquakes: analysis and field measurements. *Géotechnique* **51**, No. 5, 425-440.

Novak, M. (1991). Piles under dynamic loads: State of the art. *Proc. 2nd International conference on Recent Advances in Geotechnical Earthquake Engineering and Soil Dynamics, St. Louis*, Vol. III, 2433-2456.

Oztoprak, S. & Bolton, M.D. (2013). Stiffness of sand through a laboratory test database. *Géotechnique* **63**, No. 1, 54-70.

Randolph, M.F. & Houlsby, G.T. (1984). The limiting pressure on a circular pile loaded laterally in cohesive soil. *Géotechnique* **34**, No. 4, 613-623.

Schofield, A.N. (1980). Cambridge geotechnical centrifuge operations. *Géotechnique* **30**, No. 3, 227–268.

Viggiani, G. & Atkinson, J.H. (1995). Stiffness of fine-grained soil at very small strains. *Géotechnique* **45**, No. 2, 249-265.

Vucetic, M. & Dobry, R. (1991). Effect of soil plasticity on cyclic response. *Journal of Geotech. Eng.* **117**, No. 1, 89–117.